Journal of the European Ceramic Society **16** (1996) 187–193

0955-2219(95)00158-1
0955-2219/96/$15.00

Local Structural Information of Mullite Obtained from Diffuse X-ray Scattering

T. R. Welberry & B. D. Butler*

Research School of Chemistry, Australian National University, Canberra, ACT 0200, Australia

(Accepted 22 July 1995)

Abstract

A full reciprocal space volume of diffuse scattering data from a single crystal of the mineral mullite, $Al_2(Al_{2+2x},Si_{2-2x})O_{10-x}$, x = 0·4, has been collected. These data were analysed using least-squares techniques by writing an equation for the diffuse scattering which involves only the local order between vacancies on specific oxygen sites in the material. The effect of the large, but predictable, cation shifts on the diffuse intensity was taken account of in the coefficients to the oxygen vacancy short-range order intensities. This analysis shows that in addition to the absence of defects separated by the vectors $\frac{1}{2}$<1 1 0> and [1 1 0] (which results from the simplifying assumptions that were made), there is also a strong tendency to avoid defects separated by <0 0 1> and a moderately strong tendency to avoid pairs of defects separated by <0 0 3>, <0 1 1>, [1 –1 0] and $\frac{1}{2}$<3 1 2>. The most common inter-defect vectors found were $\frac{1}{2}$<3 1 0>, <1 0 1>, $\frac{1}{2}$<1 1 2>, <0 1 2>, $\frac{1}{2}$<1 3 0>, $\frac{1}{2}$<1 3 2> and <0 2 2>.

Introduction

Conventional crystal structure determination involves measurement of the intensities of Bragg reflections – the sharp diffraction peaks that occur at integral points of reciprocal space. Analysis using this information leads to a description of the *average* structure of the material. For a disordered material such as mullite, this may include such information as the coordinates of different atomic sites in the average unit cell, site occupancies and mean-square atomic displacements. This latter information may result from the thermal motion of the atoms or may be related to a spatial average of a static distribution in which atoms in different unit cells lie on positions distributed about the mean. Bragg-scattering thus provides only information about *single* site properties of the material. On the other hand, *diffuse X-ray scattering*, the much weaker broadly distributed scattering occurring at general points in reciprocal space, contains information concerning *pairs* of sites and is thus potentially a rich source of information regarding local chemical and displacement correlations and can be employed to aid the understanding of locally ordered materials such as mullite. Unfortunately, the extraction of correlation fields from diffuse diffraction data has proved to be a difficult task even for relatively simple systems and success in obtaining such information has mostly been limited to alloys and simple oxides (see, for example, Refs 1–3). At first sight mullite appears to be of such significantly greater complexity than these simple systems that success in extracting quantitative correlation information would seem unlikely. In this paper we describe how, by making certain simplifications based on chemical considerations, the diffuse X-ray scattering from mullite can be analysed to reveal a much more complete description of the structure than is possible from Bragg analysis.

The Average Structure

Details of the average structure of mullite of composition $Al_2(Al_{2+2x}Si_{2-2x})O_{10-x}$ where $x = 0{\cdot}4$, as revealed by the Bragg scattering,[4] are shown in Fig. 1. The structure is similar to that of sillimanite, $Al(AlSi)O_5$. Chains of edge-sharing AlO_6 octahedra, running parallel to the crystallographic **c**-axis, are crosslinked by $(Al,Si)O_4$ tetrahedra. In sillimanite the tetrahedrally coordinated cations are bridged by a single oxygen atom and are ordered in such a way that the bridging anion always connects an Si-containing tetrahedron with an Al-containing tetrahedron. In mullite some fraction, x, of these bridging oxygen sites are vacant. To preserve charge balance, each of the O^{2-} vacancies are accommodated by the exchange

*Current address: National Institute of Standards & Technology, A325 Broadway, Boulder, CO 80303, USA.

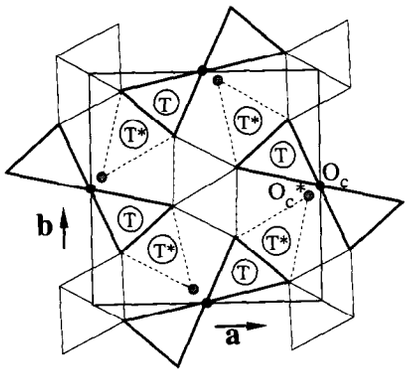

Fig. 1. The average structure of mullite seen in projection down the crystallographic **c**-axis. The sites labelled $\mathbf{O_c}$ and $\mathbf{O_c^*}$ contain oxygen atoms which bridge two or more tetrahedra. In an $x = 0{\cdot}4$ mullite the **T**, **T*** sites are disordered such that 80% of the **T** sites and 20% of the **T*** sites are occupied by Al or Si. 40% of the $\mathbf{O_c}$ sites and 20% of the $\mathbf{O_c^*}$ sites are occupied.

of $2Al^{3+}$ for $2Si^{4+}$. Because the tetrahedrally coordinated Al and Si are no longer present in the ratio of 1 : 1 these sites necessarily become chemically disordered. Furthermore, crystal structure analysis has identified the presence of a second tetrahedral site – displaced from the original by approximately 1·3 Å – that is presumably occupied by cations which have lost bridging oxygen atoms. The bridging oxygen atom was also found to occasionally occupy a site displaced 0·5 Å from its normal position and appears to be associated with the displaced tetrahedral site. In Fig. 1 the (Al,Si) tetrahedral sites are labelled **T** and **T*** and the bridging anion sites are labelled $\mathbf{O_c}$ and $\mathbf{O_c^*}$ where * indicates the displaced positions mentioned above. It should be stressed that it is only *presumed* that the **T*** sites are occupied by cations which have lost bridging oxygen atoms and that the displaced $\mathbf{O_c^*}$ sites are directly associated with them. The Bragg experiment only reveals the overall average occupancies.

The Diffuse Diffraction Data

The diffuse intensity data were collected on an instrument specially designed for the rapid collection of planar sections of single crystal diffraction patterns. The apparatus is an electronic version of a Weissenberg camera utilizing flat-cone geometry in which a curved linear (gas filled) position sensitive detector (PSD) is used to collect data normal to the Weissenberg cylinder axis. A monochromated, sealed tube, Cu K_α source is employed. With this geometry a series of scans taken as the crystal is rotated through 360° produces a flat, two-dimensional section of the diffraction pattern normal to the crystal rotation axis. Several scans can be made using different goniometer settings to construct a three-dimensional image of the diffraction space as a series of two-dimensional sections. Further details about the instrument can be found elsewhere.[5]

Although the data recorded in this way provide quantitative measurements at points in reciprocal space, it is convenient for display purposes to present the data as grey-scale images. We prefer this method to the often used practice of drawing contour plots. In Fig. 2 we show such plots of data from six different reciprocal sections. Each pattern consists of ~ 180 × 180 pixels. Each pixel corresponds to an increment in the Miller indices Δh_1, $\Delta h_2 = 0{\cdot}05$. This resolution is rather poorer than the resolution that the instrument can provide, but the data were binned at this resolution to provide a manageable number of independent measurements. Eleven sections in $\Delta h_3 = 0{\cdot}05$ increments from $h_3 = 0{\cdot}5$ to 1·0 were measured, yielding in excess of 130 000 independent measurements.

The plots of data in Fig. 2, which are all made on the same scale, demonstrate the rich detail that is present in the diffuse data. Many different features may be seen, varying from the relatively

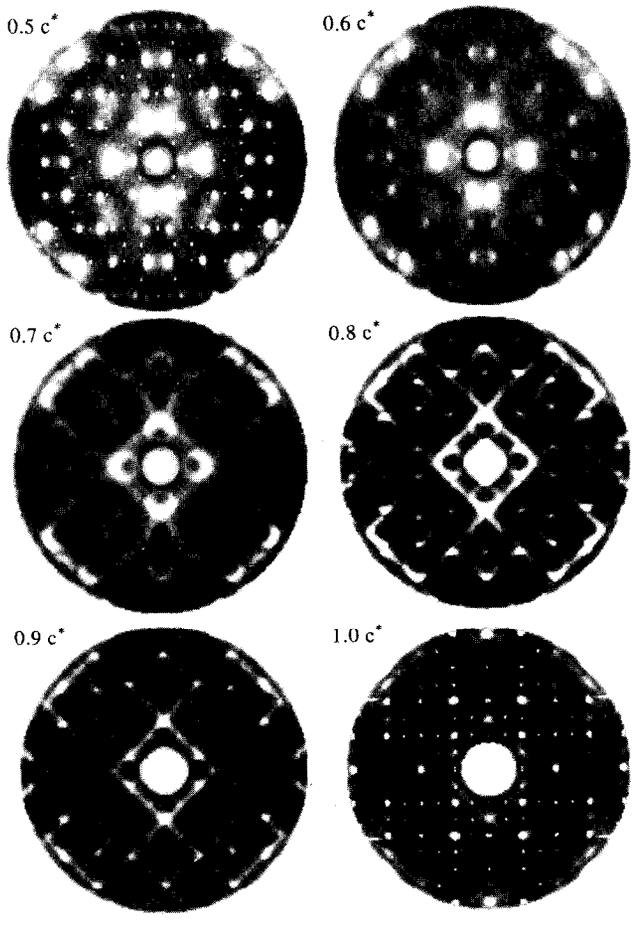

Fig. 2. Diffuse X-ray diffraction data. The data were collected digitally but are displayed on a grey scale so that the full range of diffuse features can be seen. Only six of the 11 diffuse planes that were used in the analysis are displayed. The small single pixel peaks seen in the 0·5**c*** and 1·0**c*** sections are Bragg peaks caused by $\lambda/2$ contamination of the beam.

sharp incommensurate peaks visible in the 0·5**c*** section to the more diffuse circular features in the 0·7**c*** section and the narrow lines of the 0·9**c*** section. Although in the past much interest has centred on the incommensurate peaks, these patterns reveal that these are just an integral part of the continuous diffuse distribution. The total integrated intensity in each of the different recorded sections is fairly constant.

Theory

A general description of diffuse scattering that allows for both short-range compositional (chemical) order and local atomic displacements can be obtained by expanding the exponential in the kinematic scattering equation in powers of displacement.

$$I = \sum_{n=1}^{N}\sum_{m=1}^{M} f_m f_n \exp[i\boldsymbol{k}\cdot(\boldsymbol{R}_m + \boldsymbol{u}_m - \boldsymbol{R}_n - \boldsymbol{u}_n)]$$

$$\approx \sum_{n=1}^{N}\sum_{m=1}^{M} f_m f_n \exp[i\boldsymbol{k}\cdot(\boldsymbol{R}_m - \boldsymbol{R}_n)]$$

$$\times \{1 + i\boldsymbol{k}\cdot(\boldsymbol{u}_m - \boldsymbol{u}_n) - \tfrac{1}{2}[\boldsymbol{k}\cdot(\boldsymbol{u}_m - \boldsymbol{u}_n)]^2$$

$$- \tfrac{i}{6}[\boldsymbol{k}\cdot(\boldsymbol{u}_m - \boldsymbol{u}_n)]^3 + \ldots\} \quad (1)$$

Here I is the scattered intensity and f_m is the scattering factor of the atom m associated with the lattice site at the location $\boldsymbol{R}_m$ and which is displaced from its site by a small amount $\boldsymbol{u}_m$. $\boldsymbol{k} = h_1\boldsymbol{a}^* + h_2\boldsymbol{b}^* + h_3\boldsymbol{c}^*$ is the scattering vector. Eqn (1) expresses the fact that the intensity distribution may be written as the sum of component intensities: the first term being independent of the displacements, the second term dependent on the first moment of displacements, the third term on the second moment, etc.

$$\mathbf{I}_{\text{Diffuse}} \approx \mathbf{I}_0 + \mathbf{I}_1 + \mathbf{I}_2 + \mathbf{I}_3 + \ldots \quad (2)$$

It is usual in analyses of alloys and simple oxides to truncate this Taylor expansion at second order, although recently we have shown that for cubic-stabilized zirconias the third and higher order terms are also important. These components can be shown to have the following forms,

$$\mathbf{I}_0 = -\sum_{ij}\sum_{lmn} c_i c_j f f_j^* \alpha_{lmn}^{ij} \cos\{2\pi(h_1 l + h_2 m + h_3 n)\} \quad (3)$$

$$\mathbf{I}_1 = -2\pi \sum_{ij}\sum_{lmn} c_i c_j f f_j^* (1 - \alpha_{lmn}^{ij})[h_1 \langle X_{lmn}^{ij}\rangle + h_2\langle Y_{lmn}^{ij}\rangle + h_3\langle Z_{lmn}^{ij}\rangle]$$
$$\times \sin\{2\pi(h_1 l + h_2 m + h_3 n)\} \quad (4)$$

$$\mathbf{I}_2 = -2\pi^2 \sum_{ij}\sum_{lmn} c_i c_j f f_j^* (1 - \alpha_{lmn}^{ij})$$
$$\times [h_1^2\{\langle (X_{lmn}^{ij})^2\rangle - (1 - \alpha_{lmn}^{ij})^{-1}\langle (X_{\infty}^{ij})^2\rangle\}$$
$$+ h_2^2\{\langle (Y_{lmn}^{ij})^2\rangle - (1 - \alpha_{lmn}^{ij})^{-1}\langle (Y_{\infty}^{ij})^2\rangle\}$$
$$+ h_3^2\{\langle (Z_{lmn}^{ij})^2\rangle - (1 - \alpha_{lmn}^{ij})^{-1}\langle (Z_{\infty}^{ij})^2\rangle\}$$
$$+ 2h_1h_2\{\langle X_{lmn}^{ij} Y_{lmn}^{ij}\rangle + 2h_1h_3\langle X_{lmn}^{ij} Z_{lmn}^{ij}\rangle$$
$$+ 2h_2h_3\{\langle Y_{lmn}^{ij} Z_{lmn}^{ij}\rangle]$$
$$\times \cos\{2\pi(h_1 l + h_2 m + h_3 n)\} \quad (5)$$

The first term $\mathbf{I}_0$ is the intensity component due to short-range order and is not dependent on displacements. There is one term in this summation for every different interatomic vector *lmn* along which significant correlation may be present. Each term in the sum involves a short-range order parameter, α_{lmn}^{ij}, defined by

$$\alpha_{lmn}^{ij} = 1 - P_{lmn}^{ij}/c_j \quad (6)$$

where P_{lmn}^{ij} is the conditional probability of finding an atom with label j at the end of a vector $\boldsymbol{r}_{lmn}$ given that there is an atom with label i at its origin. $\mathbf{I}_1$ and $\mathbf{I}_2$, which involve displacements, similarly also have terms for every different interatomic vector. For a simple binary system $\mathbf{I}_1$ has six terms for each interatomic vector and $\mathbf{I}_2$ has 18. Fitting equations of this form with such large numbers of parameters is a formidable task even for simple systems, but for a system as complex as mullite it is quite prohibitive. Consequently we look for a means by which the problem may be simplified.

A Simplified Model

The simplification we adopt consists of making two assumptions. First we assume that only the distribution of oxygen vacancies is important, and that the shift of cations from the **T** to the **T*** sites and the shift of the oxygens from $\mathbf{O}_c$ to $\mathbf{O}_c^*$ follow from these as a direct consequence [see Fig. 3(a)]. Secondly, we assume that certain local configurations, which are chemically implausible, do not occur at all in the structure. These are shown in Figs 3(b) and 3(c). In Fig. 3(b) the presence of two vacancies separated by $\frac{1}{2}\langle 1\,1\,0\rangle$ causes the cation 'M' to have no bridging oxygen atom to bond with. In Fig. 3(c) the presence of two vacancies separated by [1 1 0] causes four tetrahedral cations to share the same bridging oxygen.

A description of the mullite structure based on the occupancy of the bridging oxygen sites alone can then be formulated as follows. When a bridging

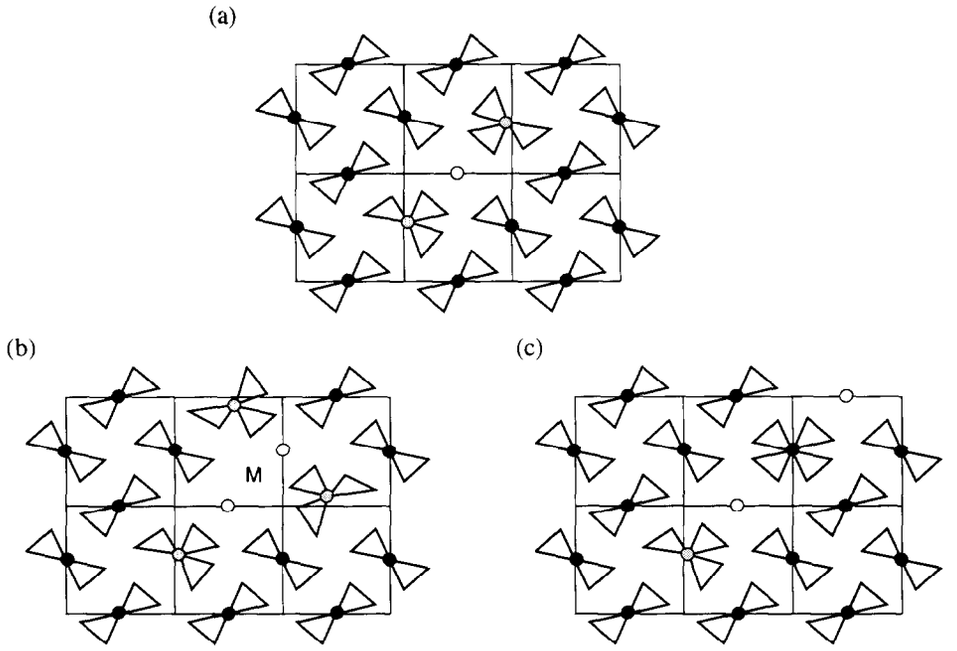

Fig. 3. In all the figures a black circle represents an oxygen atom on the $\mathbf{O}_c$ site, a grey circle an oxygen atom on the $\mathbf{O}_c^*$ site and an open circle represents a vacancy. (a) Shows the effect of introducing an oxygen vacancy into the mullite structure. Two nearby cations transfer from **T** sites to the alternative **T*** sites and the two $\mathbf{O}_c$ oxygens, which now are bonded to three cations, move to the $\mathbf{O}_c^*$ sites. (b) and (c) Show two configurations that are assumed never to occur in the disordered structure. In (b) the cation 'M' is left without a bridging $\mathbf{O}_c$ atom to bond with. In (c) four cations are forced to share one bridging oxygen.

site is occupied by an oxygen atom we 'decorate' that site with one $\mathbf{O}_c$ oxygen atom and two **T** cations. When the site is vacant we decorate with two **T*** cations, two neighbouring $\mathbf{O}_c^*$ oxygen atoms and *subtract* two neighbouring $\mathbf{O}_c$ oxygen atoms. Note that as long as the ordering rules stated above are obeyed and all the bridging sites have been 'filled' with either an oxygen atom or a vacancy, the positions of all tetrahedrally coordinated cations and all of the bridging oxygen atoms will have been specified. The 'negative' $\mathbf{O}_c$ oxygen atoms that are included with an oxygen vacancy are used as a means to displace $\mathbf{O}_c$ atoms from their normal positions to positions labelled $\mathbf{O}_c^*$ while still preserving the total number of oxygen atoms in the crystal. Once the entire lattice has been decorated in this way there will be no remaining 'negative' oxygen atoms.

With this formulation we can discard the intensity components, $\mathbf{I}_1$ and $\mathbf{I}_2$, and use only the short-range order (SRO) term $\mathbf{I}_0$, in which we replace the atomic scattering factor by structure factors for the chemical motifs of an occupied or a vacant site. This simplification merely incorporates the displacements which would normally appear in $\mathbf{I}_1$ and $\mathbf{I}_2$ into $\mathbf{I}_0$, but in doing so automatically dictates that the displacements when they occur are always of exactly the same magnitude. The scattering power of an occupied (O) and vacant (V) $\mathbf{O}_c$ site can be calculated as a simple structure factor of the chemical motifs described above:

$$F_O^1 = f_O + 2f_{Al}\cos\{2\pi(x_T h_1 + y_T h_2)\}$$
$$F_V^1 = 2f_O\cos\{2\pi(x_{O_c^*} h_1 + y_{O_c^*} h_2)\} + 2f_{Al}\cos\{2\pi(x_{T^*} h_1 + y_{T^*} h_2)\} - 2f_O\cos\{2\pi(x_{O_c} h_1 + y_{O_c} h_2)\} \quad (7)$$

Here, f_O, f_{Al} are the atomic scattering factors of O and Al; x_T, y_T etc. are the fractional coordinates of the **T**, **T***, $\mathbf{O}_c$ and $\mathbf{O}_c^*$ sites measured relative to the $\mathbf{O}_c$ site in question; h_1, h_2, h_3 are continuous reciprocal space coordinates; and the superscript on the structure factors indicates the sublattice upon which the oxygen atom or vacancy resides. Sublattice 1 refers to the $\mathbf{O}_c$ site at $(\frac{1}{2}0\frac{1}{2})$ and translationally equivalent sites, while sublattice 2 refers to the $\mathbf{O}_c$ site at $(0\frac{1}{2}\frac{1}{2})$. Equation (7) gives the expressions for motifs centred at sites on sublattice 1. Similar, symmetry-related, expressions may be written for motifs centred on sublattice 2.

Replacing the atomic scattering factors in Eqn (3) by the structure factors of the chemical motifs we obtain, after some manipulation (see Butler & Welberry[6] for further details), the following expression for the SRO diffuse scattering in mullite:

$$I_{SRO}^{mullite} = \mu_1 I_1 + \mu_2 I_2 + \mu_{12} I_{12} \quad (8)$$

where

$$I_1 = \sum_{\substack{lmn \\ l,\, m,\, n \text{ integer}}} \alpha_{lmn}^{O_1 V_1} \cos(h_1 l + h_2 m + h_3 n)$$

$$I_2 = \sum_{\substack{lmn \\ l,\, m,\, n \text{ integer}}} \alpha_{lmn}^{O_2V_2} \cos(h_1 l + h_2 m + h_3 n)$$

$$I_{12} = \sum_{\substack{lmn \\ l = \text{int} + 1/2 \\ m = \text{int} + 1/2 \\ n = \text{int}}} \alpha_{lmn}^{O_1V_2} \cos(h_1 l + h_2 m + h_3 n) \qquad (9)$$

and,

$$\mu_1 = c_O c_V (F_{O_1} - F_{V_1})^2$$

$$\mu_2 = c_O c_V (F_{O_2} - F_{V_2})^2$$

$$\mu_{12} = 2 c_O c_V \Re e\{(F_{O_1} - F_{V_2})(F_{O_2} - F_{V_2})^*\} \qquad (10)$$

The three intensities, I_1, I_2, and I_{12}, are periodic functions in reciprocal space with a repeat that is commensurate with the first Brillouin zone and the coefficients μ_1, μ_2 and μ_{12} are continuous functions in reciprocal space. I_1 and I_2 involve only correlations between sites on the same sublattice (1 and 2 respectively), while I_{12} involves cross-correlations between the two different sublattices. In Fig. 4 we show plots of the functions, μ_1, μ_2, μ_{12}, which are calculated from the fractional coordinates of the average structure obtained from the Bragg reflections. It should also be noted that since **T**, **T***, $\mathbf{O_c}$ and $\mathbf{O_c^*}$ all have the same z-coordinate in the structure, the functions μ_1, μ_2 and μ_{12} are virtually independent of h_3, the reciprocal coordinate in the **c***-direction. The variation of the intensity distribution with reciprocal section thus results entirely from the Warren short-range order parameters, α_{lmn}, appearing in the three intensity components I_1, I_2 and I_{12}.

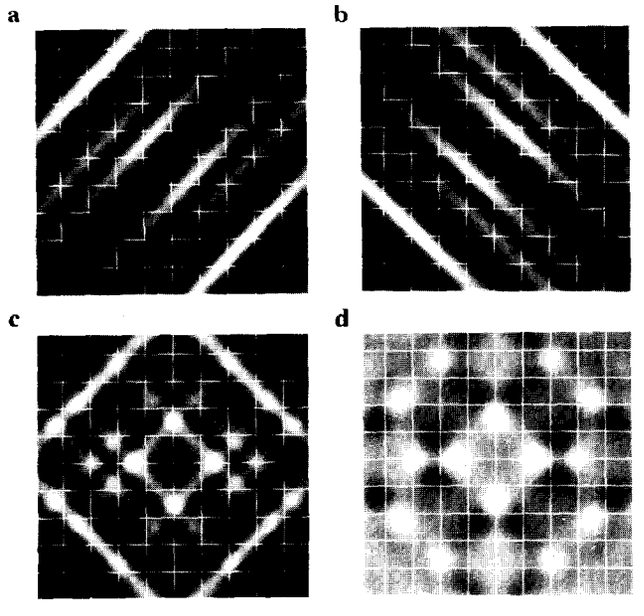

Fig. 4. Plots in the $(hk0)$ plane of the coefficients μ_1, μ_2 and μ_{12} which occur in Eqn (8). These coefficients are constant functions calculated from the coordinates obtained from the average structure analysis. (a) μ_1. (b) μ_2. (c) $\mu_1 + \mu_2$. (d) μ_{12}. μ_1 and μ_2 are positive everywhere but μ_{12} varies from negative (black) to positive (white). The white lines drawn on the figures indicate where h_1 and h_2 are integral.

Results

A value for each of the three intensity components can be obtained for a given point inside the first Brillouin zone by gathering together several measurements of the diffuse intensity from points in the reciprocal space that are related by symmetry with this point. The set of measurements related by symmetry in this way is commonly referred to as an *associated set* and the point inside the minimum repeat volume is referred to as a *minimum volume point.*[7] For example, if the point (h_1, h_2, h_3), lies inside the first Brillouin zone, then the points $(1 - h_1, h_2, h_3)$, $(h_1, 2 + h_2, h_3)$, $(2 + h_1, 3 - h_2, 1 + h_3)$, etc. form the associated set of the minimum volume point (h_1, h_2, h_3). Each of the intensity components I_1, I_2 and I_{12} have the same numerical magnitude (but not necessarily sign) for all points inside a particular associated set but the coefficients μ_1, μ_2 and μ_{12} vary predictably in a way that does not repeat commensurately with the underlying reciprocal lattice. Any collection of three or more measurements in an associated set can therefore be used to solve for the three intensity components at one minimum volume point. In the present case, upwards of 30–40 measurements were available in each associated set and with only three intensity components to solve for the problem is highly overdetermined. Standard least-squares procedures were used to solve for the three intensity components at each of 1331 points in the minimum volume.

When this had been done for every point in the minimum volume, the Warren short-range order parameters α_{lmn} were extracted from each of the three component intensities by simple Fourier inversion of Eqn (9). The most significant of these are given in Table 1. Assuming that the three SRO intensities derived this way are the only significant

Table 1. Local order parameters for mullite determined from the least-squares analysis

Interatomic vector, lmn	*Short-range order parameter*, α_{lmn}	*Interatomic vector*, lmn	*Short-range order parameter*, α_{lmn}
$\frac{1}{2}$<1 1 0>	−0·250	<0 1 1>	−0·122
[1 1 0]	−0·250	[1 1 1]	−0·079
[1 −1 0]	−0·081	[1 −1 1]	+0·000
<0 0 1>	−0·227	$\frac{1}{2}$<1 1 2>	+0·109
<1 0 0>	−0·004	$\frac{1}{2}$<3 1 0>	+0·141
<0 1 0>	+0·015	$\frac{1}{2}$<1 3 0>	+0·077
<0 0 2>	−0·019	$\frac{1}{2}$<3 1 2>	−0·092
<0 0 3>	−0·124	$\frac{1}{2}$<1 3 2>	+0·058
<0 0 4>	+0·047	<0 1 2>	+0·088
<1 0 1>	+0·113	<0 2 2>	+0·051

contributions to the total diffuse intensity in mullite, then the oxygen-vacancy SRO parameters obtained by this procedure will contain all the information that the diffuse part of the diffraction pattern can provide.

The intensity R factor

$$R = [\sum(I_{obs} - I_{calc})^2/\sum I_{calc}^2]$$

for a typical least-squares solution of one of the 1331 minimum volume points was approximately 35%. This obvious quantitative discrepancy may seem very high by conventional crystallographical standards but the resulting least-squares fit is not as bad as this figure implies. When all 1331 independent solutions are used, together with the μ_1, μ_2, μ_{12} coefficients, to obtain a 'best-fit' calculated diffraction pattern for visual comparison with the observed patterns, the results are really rather convincing (see Fig. 5).

Both Figs 2 and 5 are reproduced on the same scale so that the grey shades can be compared to see how the two agree. There are a few obvious differences. For instance, in the 0·7**c*** reciprocal layer the measured intensities near the origin and at large scattering angles are noticeably higher than in the calculated pattern, whereas at intermediate angles this situation is reversed. There are also distinct diagonal dark bands visible in the 0·5**c*** layer of the calculated pattern that are much less distinct in the data. These differences may indicate minor short-comings in the model used to derive Eqn (8) which does not allow for atom displacements other than those included in the simple chemical motifs described.

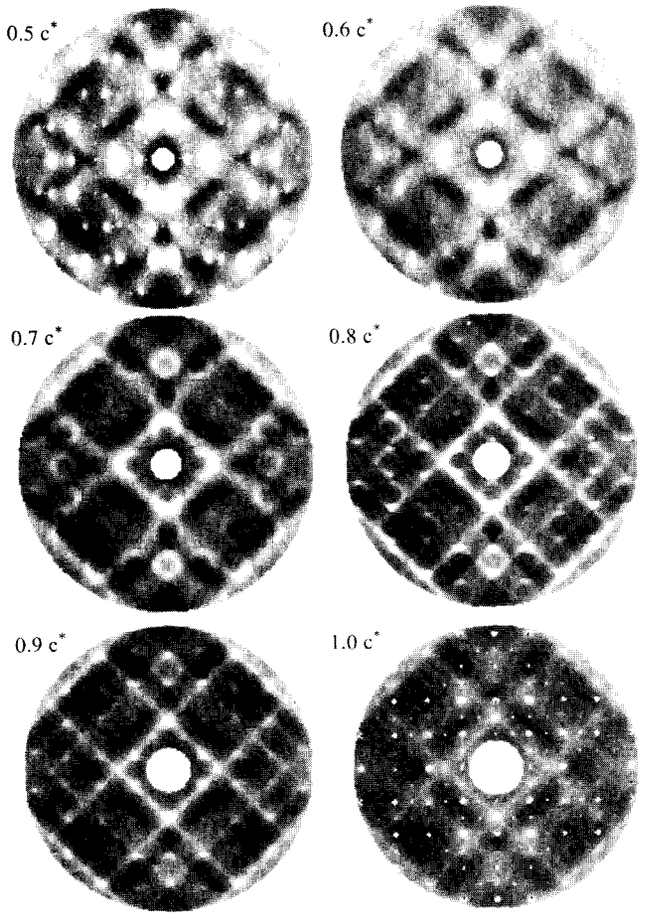

Fig. 5. Diffraction patterns calculated from the least-squares fit of the model to the observed data. The least-squares solution provided three intensity components at each of 1331 points inside the first Brillouin zone. The entire pattern was generated by multiplying these component intensities by the appropriate coefficients μ_1, μ_2, μ_{12} and adding.

The most significant values for the Warren short-range order parameters, α_{lmn}, obtained from the analysis are shown in Table 1. For a vacancy concentration of 0·2 the most negative value of α_{lmn} feasible is $\alpha_{lmn} = -0{\cdot}25$, which corresponds to complete avoidance of defect pairs separated by the vector *lmn*. Thus we see that, in addition to the absence of defects separated by the vectors $\frac{1}{2}$<1 1 0> and [1 1 0] (which results from the simplifying assumptions that were made), there is also a strong tendency to avoid defects separated by <0 0 1> and a moderately strong tendency to avoid pairs of defects separated by <0 0 3>, <0 1 1>, [1 −1 0] and $\frac{1}{2}$<3 1 2>. The most common inter-defect vectors found were <1 0 1>, $\frac{1}{2}$<1 1 2> and $\frac{1}{2}$<3 1 0>.

Conclusion

Comparison of Figs 2 and 5 demonstrates convincingly that, for this seemingly complicated mineral, the diffuse scattering can be described simply as the sum of three component short-range order diffuse intensities. Two of these components involve correlations between the basic defects on each of the two different sublattices (symmetry-related) and the third involves correlations between the two sublattices. Although there are quantitative discrepancies indicating some short-comings in the fine detail of the model, there is no doubt that the model is essentially correct.

The basic defect consists of a vacant $\mathbf{O}_c$ site together with a transfer of its two neighbouring tetrahedral cations from a **T** to a **T*** site. Each **T*** cation then shares a further bridging oxygen which shifts from $\mathbf{O}_c$ to $\mathbf{O}_c^*$ [see Fig 3(a)]. An integral part of the model was the necessity to assume that two chemically implausible configurations [shown in Figs 3(b) and 3(c)] were forbidden. If two defects were separated by $\frac{1}{2}$[1 1 0] the intervening cation would be left without a bridging $\mathbf{O}_c$ atom, while if two defects were separated by [1 1 0] it would be necessary for four cations to share the same bridging $\mathbf{O}_c$ atom. The analysis revealed that defect pairs separated by <0 0 1> were strongly avoided, and that defects separated by <0 0 3>,

<011>, [1–10] or $\frac{1}{2}$<312> also tended to be avoided, although rather less strongly. The most common inter-defect vectors found were $\frac{1}{2}$<310>, <101>, $\frac{1}{2}$<112>, <012>, $\frac{1}{2}$<130>, $\frac{1}{2}$<132> and <022>.

References

1. Hayakawa, M. & Cohen, J. B., *Acta Crystallogr.*, **A31** (1975) 635–45.
2. Matsubara, E. & Cohen, J. B., *Acta Metall.*, **33** (1985) 1945–55.
3. Reinhard, L., Robertson, J. L., Moss, S. C., Ice, G. E., Zschack, P. & Sparks, C. J., *Phys. Rev. B*, **45** (1992) 2662–76.
4. Angel, R. J. & Prewitt, T., *Am. Mineral*, **71** (1986) 1476–82.
5. Osborn, J. C. & Welberry, T. R., *J. Appl. Crystallogr.*, **23** (1990) 476–84.
6. Welberry, T. R. & Butler, B. D., *J. Appl. Crystallogr.*, **27** (1994) 742–54.
7. Wu, T. B., Matsubara, E. & Cohen, J. B., *J. Appl. Crystallogr.*, **16** (1983) 407–14.